

Self-consistent model for dust-gas coupling in protoplanetary disks

Konstantin Batygin¹  and Alessandro Morbidelli²

¹ Division of Geological and Planetary Sciences, California Institute of Technology, Pasadena, CA 91125, USA
e-mail: kbatygin@gps.caltech.edu

² Laboratoire Lagrange, Université Côte d'Azur, Observatoire de la Côte d'Azur, CNRS, CS 34229, 06304 Nice, France
e-mail: alessandro.morbidelli@oca.eu

Received 25 January 2022 / Accepted 28 March 2022

ABSTRACT

Various physical processes that ensue within protoplanetary disks – including vertical settling of icy and rocky grains, radial drift of solids, planetesimal formation, as well as planetary accretion itself – are facilitated by hydrodynamic interactions between H/He gas and high-Z dust. The Stokes number, which quantifies the strength of dust-gas coupling, thus plays a central role in protoplanetary disk evolution and its poor determination constitutes an important source of uncertainty within the theory of planet formation. In this work, we present a simple model for dust-gas coupling and we demonstrate that for a specified combination of the nebular accretion rate, \dot{M} , and turbulence parameter α , the radial profile of the Stokes number can be calculated in a unique way. Our model indicates that the Stokes number grows sublinearly with the orbital radius, but increases dramatically across the water-ice line. For fiducial protoplanetary disk parameters of $\dot{M} = 10^{-8} M_{\odot}$ per year and $\alpha = 10^{-3}$, our theory yields characteristic values of the Stokes number on the order of $St \sim 10^{-4}$ (corresponding to \sim mm-sized silicate dust) in the inner nebula and $St \sim 10^{-1}$ (corresponding to icy grains of a few cm in size) in the outer regions of the disk. Accordingly, solids are expected to settle into a thin subdisk at large stellocentric distances, while remaining vertically well mixed inside the ice line.

Key words. planets and satellites: formation – protoplanetary disks

1. Introduction

All planets originate as dust, embedded within protoplanetary disks. As such, the physical properties and radial distribution of solid material within circumstellar nebulae play a key role in determining the efficiency of planetesimal formation (Youdin & Goodman 2005; Johansen & Youdin 2007), the principal mode of planetary accretion (Ormel and Klahr 2010; Lambrechts and Johansen 2012), as well as the large-scale architecture of the emergent planetary system (Kokubo and Ida 2012; Bitsch et al. 2019). In other words, the overall process of planetary conglomeration is inherently controlled by the interactions between dust particles and the hydrogen-helium fluid that comprises the dominant component of the disk.

The degree of coupling between dust and gas is quantified by a dimensionless quantity – the Stokes number¹. In the context of astrophysical disks, the Stokes number specifies the fraction of an orbit that is required for a grain to re-equilibrate with the (sub-Keplerian) flow of the gas (e.g., Adachi et al. 1976; Weidenschilling 1977). Because the Stokes number depends both upon local disk properties and the particle size, disparate approaches to computing its value lead to considerable (and model-specific) degeneracies (Chiang & Youdin 2010; Lambrechts et al. 2019; Laibe et al. 2020 and references therein). Therefore, establishing a connection between the Stokes number and local properties of the nebula is key to

alleviating an important source of uncertainty in the theory of planet formation.

In this work, we demonstrate that the Stokes number that is attainable by solid particles cannot be divorced from the disk model. We outline a simple theoretical model and we self-consistently compute the radial profile of the Stokes number within the young protoplanetary nebulae. The compositional dependence of the dust fragmentation threshold – and by extension, the water-ice sublimation line – plays a key role in our analysis. Informed by laboratory experiments, we assume that icy grains are “stickier” than refractory particles. This distinction translates into corresponding fragmentation velocities that differ by an order of magnitude and facilitates the main difference in the strength of dust-gas coupling between the silicate-rich inner disk and the ice-dominated outer disk.

We begin our calculation by recalling the basic properties of accretion disks in Sect. 2. We compute the Stokes number itself in Sect. 3. The direct implications of our model are presented in Sect. 4. We summarize and discuss our results in Sect. 5.

2. Disk model

An essential property of protoplanetary disks is that they accrete onto their host stars. At any orbital radius, r , the relationship between the mass-accretion rate, \dot{M} , and the disk surface density, Σ , is given by (e.g., Armitage 2010):

$$\dot{M} = |2\pi r v_r \Sigma|. \quad (1)$$

A conventional assumption of a steady-state disk is obtained by supposing that \dot{M} is independent of r . Within the framework of

¹ Defined as the product of the frictional timescale and the orbital frequency, the Stokes number is also referred to in the literature as the “dimensionless stopping time”.

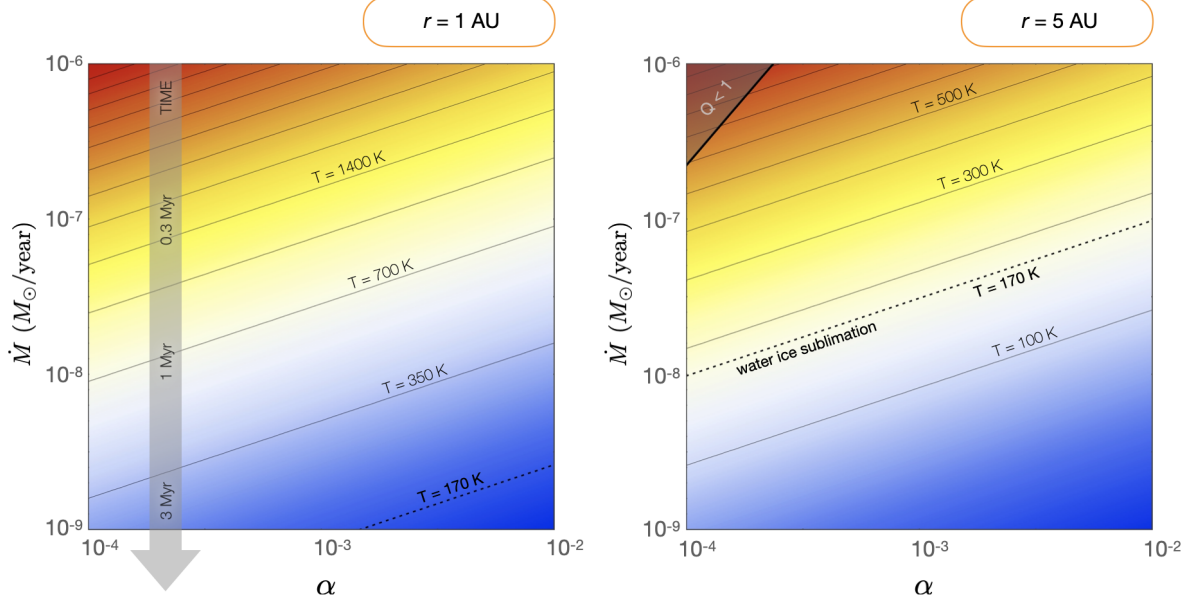


Fig. 1. Mid-plane temperature within the model (active) accretion disk at orbital radii of $r = 1$ AU (left panel) and $r = 5$ AU (right panel). Contours are shown on the \dot{M} – α plane, spanning the range of parameters relevant to young protoplanetary nebulae. Level curves corresponding to the assumed water ice sublimation temperature of $T_{\text{ice}} = 170$ K are shown with dashed lines. As disks evolve, their accretion rates diminish, meaning that \dot{M} constitutes a proxy for time, as shown on the left panel. A small region of gravitationally unstable parameter space where Toomre $Q < 1$ is labeled on the top-left corner of the right panel.

the viscous accretion paradigm (Lynden-Bell and Pringle 1974), the radial velocity of the gas, v_r , arises from subsonic turbulence within the system. Adopting the conventional (Shakura & Sunyaev 1973) prescription for turbulent viscosity, $\nu = \alpha c_s h$, we have:

$$v_r = -\frac{3}{2} \frac{\nu}{r} = -\frac{3 \alpha k_b T}{2 \mu r \Omega}, \quad (2)$$

where μ is the mean molecular weight, k_b is the Boltzmann constant, and Ω is the orbital frequency. Notice that in the above expression we have used the standard relation between the speed of sound and temperature $c_s = \sqrt{k_b T / \mu}$, and have expressed the disk scale height as $h = c_s / \Omega$.

The functional form of the mid-plane temperature of an actively heated optically thick disk stems from balance between viscous heat generation within the nebula and radiative losses (e.g., Lee et al. 1991):

$$\sigma_{\text{sb}} T^4 = \frac{9 \dot{M} \tau \Omega^2}{32 \pi}, \quad (3)$$

where σ_{sb} is the Stefan-Boltzmann constant, and τ is the optical depth. Assuming that dust acts as the dominant source of opacity, the optical depth can be expressed as (Bitsch et al. 2014):

$$\tau = \frac{1}{2} f_{\text{dust}} \Sigma \kappa_{\text{dust}}, \quad (4)$$

where $f_{\text{dust}} \approx 0.01$ is the dust-to-gas ratio and $\kappa_{\text{dust}} \approx 30 \text{ m}^2 \text{ kg}^{-1}$ (for simplicity, here we neglect the temperature-dependence; Bell and Lin 1994).

Combining these relations, we obtain an expression for the mid-plane temperature profile of the disk as a function of \dot{M} and α :

$$T = \left(\frac{3 f_{\text{dust}} \kappa_{\text{dust}} \mu \Omega^3 \dot{M}^2}{64 \pi^2 k_b \sigma_{\text{sb}} \alpha} \right)^{1/5}. \quad (5)$$

As an illustrative example, the left and right panels of Fig. 1 show level curves of the mid-plane temperature on the α – \dot{M} plane, at $r = 1$ AU and 5 AU, respectively. Additionally, on the left panel of the figure, \dot{M} is linked with disk age using the \dot{M} – age relationship presented by Hartmann et al. (1998). Because the mid-plane temperature determines the speed of sound and the pressure scale-height of the disk, a given combination of α and \dot{M} also uniquely specifies the profile of the disk viscosity.

3. Stokes number

The physical interpretation of the Shakura-Sunayev α is nothing more than the square of the turbulent Mach number (or equivalently, the ratio of stress to pressure). Correspondingly, the characteristic velocity scale at which turbulent eddies manifest within the nebula is $v_{\text{turb}} \sim \sqrt{\alpha} c_s$. Turbulent fluctuations within the gas give rise to a dispersion of velocities among the dust grains, such that particles that are coupled to the gas (i.e., those with Stokes number, St , of unity or smaller) will experience collisions with velocities that are approximately given by (Birnstiel et al. 2009):

$$\sigma_{\text{dust}} \sim \sqrt{\text{St}} v_{\text{turb}} = \sqrt{\alpha \text{St}} c_s. \quad (6)$$

We note that herein we have assumed that turbulent diffusivity of the gaseous and solid components of the disk are equivalent. In other words, our analysis was carried out based on a turbulent Schmidt number of $\text{Sc} = 1$. Generalizations of our results with regard to any other value of the Schmidt number can be done by introducing a second turbulence parameter $\alpha' = \alpha / \text{Sc}$ related to the dust subdisk.

A generic barrier to particle growth within the disk is presented by fragmentation and experimental data indicate a fragmentation velocity of $v_f^{\text{rock}} \approx 1 \text{ m s}^{-1}$ and $v_f^{\text{ice}} \approx 10 \text{ m s}^{-1}$ and for

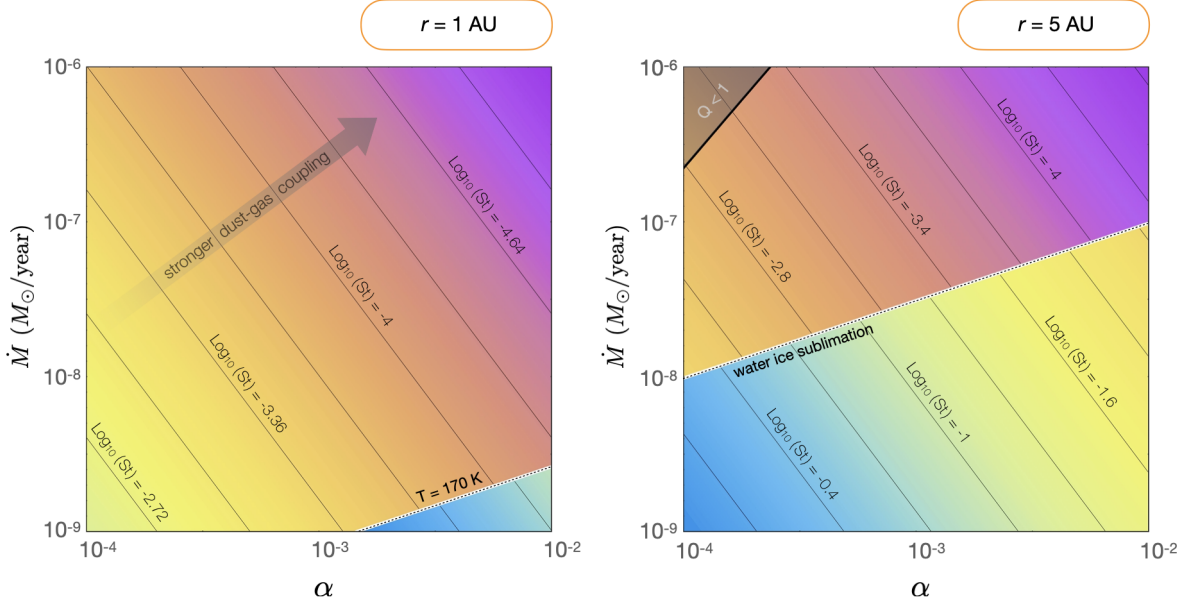


Fig. 2. Stokes number attainable by dust grains at $r = 1$ AU (left panel) and $r = 5$ AU (right panel). Owing to the fragmentation barrier, solid grains within the disk cannot grow to an arbitrarily large size and disk turbulence acts as a limiting mechanism for particle growth. The inner regions of the disk are characterized by Stokes numbers on the order of $St \sim 10^{-4}$, indicating very tight gas-dust coupling. Conversely, icy grains within the outer disk can reach Stokes numbers of order $St \sim 10^{-1}$, implying diminished aerodynamic drag.

silicate and water-ice particles, respectively² (Blum and Münch 1993; Stewart & Leinhardt 2009). An equivalence between the fragmentation speed and the dust velocity dispersion thus yields a maximal Stokes number that grains can achieve within the nebula:

$$St_{\max} = \frac{1}{3} \frac{v_f^2}{\alpha c_s^2}, \quad (7)$$

where the numerical factor of $1/3$ arises from a somewhat more detailed analysis (Ormel & Cuzzi 2007; Birnstiel et al. 2012). Of course, in a realistic disk, dust particles follow a distribution of sizes, which translates to a range of relevant Stokes numbers. Nevertheless, the relatively rapid rate of growth of solid grains within the nebula³ is likely to ensure that the characteristic value of St is close to its maximal threshold. Consequently, for the remainder of the paper, we assume that $St \sim St_{\max}$.

Substituting results from the previous section, we obtain the Stokes number as a function of α and \dot{M} :

$$St = \frac{2 v_f^2}{3} \left(\frac{2 \pi^2 \sigma_{\text{sb}} \mu^4}{3 k_b^4 f_{\text{dust}} \kappa_{\text{dust}} \dot{M}^2 \alpha^4 \Omega^3} \right)^{1/5}. \quad (8)$$

Drawing a parallel with Fig. 1, in Fig. 2 we project contours of the Stokes number onto the $\alpha - \dot{M}$ plane at $r = 1$ AU and $r = 5$ AU, assuming a H_2O condensation temperature of $T_{\text{ice}} = 170$ K. We note that for equivalent (and characteristic) values of viscosity and accretion rate (e.g., $\alpha \sim 10^{-3}$, $\dot{M} \sim 10^{-8} M_{\odot} \text{ yr}^{-1}$), at $r = 1$ AU and $r = 5$ AU, we obtain $St \sim 2 \times 10^{-4}$ and $St \sim 10^{-1}$, respectively, implying very strong dust-gas coupling in the inner disk but only marginal coupling in the outer disk.

² We note that recent literature points to an additional temperature-dependence of v_f for $T \ll T_{\text{ice}}$ and for $T \sim T_{\text{Si}}$ (Musiolik & Wurm 2019; Pillich et al. 2021), which we neglect for simplicity.

³ Particle growth timescale is well-approximated by $\tau_{\text{grow}} \sim 1/(\mathcal{Z} \Omega)$, where \mathcal{Z} is the metallicity (Drażkowska et al. 2016).

The overall functional form of Eq. (8) indicates that the Stokes number scales as the orbital radius to the power of nineteen-tenths and therefore increases in a marginally sub-linear manner with stellocentric distance. Moreover, the results depicted in Fig. 2 highlight the importance of the water-ice line as a transition point within the disk, beyond which the value of the Stokes number increases dramatically due to the increase in v_f . To illustrate the dependence of St on disk parameters, in Fig. 3, we show St as a function of r for various accretion rates and disk viscosity parameters of $\alpha = 10^{-3}$ (top panel) and $\alpha = 10^{-4}$ (bottom panel).

4. Results

A number of immediate implications follow from Eq. (8), and in this section, we extend our model to compute the efficiency of vertical settling as well as the rate of radial drift of the dust. Additionally, we convert our estimates of St into a distribution of particle sizes within a protoplanetary disk and use our results to delineate the characteristic regimes of pebble accretion as a function of orbital radius as well as planet-to-star mass ratio. For the following calculations, we adopted a nominal combination of turbulence and accretion-rate parameters of $\alpha = 10^{-3}$ and $\dot{M} \sim 10^{-8} M_{\odot} \text{ yr}^{-1}$, which yield a model disk that is somewhat less massive than (but nevertheless comparable to) the Hayashi (1981) minimum mass solar nebula.

Owing to a balance between turbulent stirring and gravitational settling, dust grains within the nebula form an embedded solid subdisk with a scale-height h_{\bullet} . In general, the scale-height of the dust cannot exceed the scale height of the gas and it is convenient to consider the normalized quantity⁴ h_{\bullet}/h (Dubrulle et al. 1995):

$$\frac{h_{\bullet}}{h} = \frac{1}{\sqrt{1 + St/\alpha}}. \quad (9)$$

⁴ As in Eq. (6), in Eq. (9), we have assumed a turbulent Schmidt number of unity.

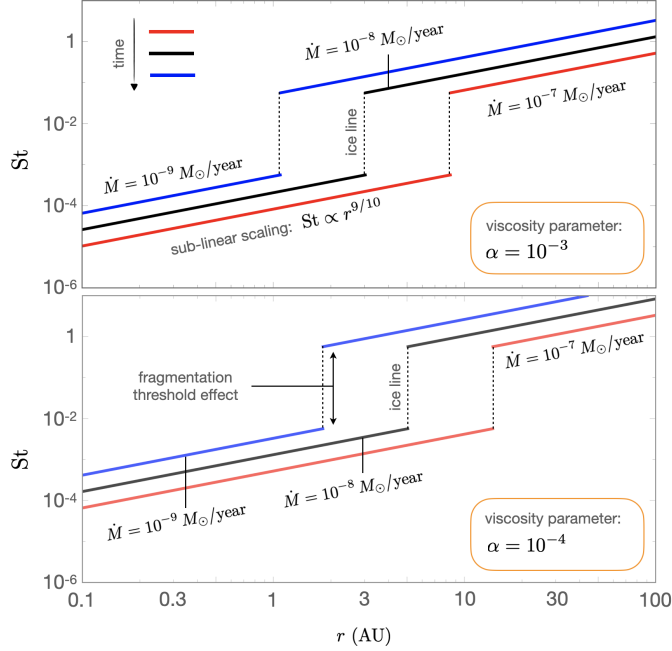


Fig. 3. Stokes number as a function of the orbital radius for Shakura-Sunayev $\alpha = 10^{-3}$ (top panel) and $\alpha = 10^{-4}$ (bottom panel). Both panels show curves corresponding to disk accretion rates of $\dot{M} = 10^{-7} M_{\odot} \text{ yr}^{-1}$ (red), $10^{-8} M_{\odot} \text{ yr}^{-1}$ (black), and $10^{-9} M_{\odot} \text{ yr}^{-1}$ (blue). Despite being quantitatively distinct, each profile is characterized by a $\text{St} \propto r^{9/10}$ scaling, as well as a dramatic (factor of ~ 100) increase in St across the ice sublimation front, owing to a change in the fragmentation threshold.

A profile of h_{\bullet}/h as a function of r is shown as a gray curve in the top panel of Fig. 4. We call attention to the fact that in the inner disk, $\text{St} \ll \alpha$, and h_{\bullet}/h tends towards unity, implying a well-mixed particle layer. Conversely, in the outer disk, $\text{St} \gg \alpha$, and the solid subdisk settles to a normalized thickness of $h_{\bullet}/h \approx \sqrt{\alpha/\text{St}} \lesssim 0.1$. Notwithstanding the definitive nature of these results, it is important to keep in mind that real protoplanetary disks will always host particles with Stokes numbers that are substantially smaller than that given by Eq. (8) in some (presumably small) proportion. In other words, even in a physical regime where $h_{\bullet}/h \ll 1$, very small (e.g., \sim micron-sized) grains will remain vertically well-mixed and continue to reside within the upper layers of protoplanetary nebulae (Laibe et al. 2020).

The radial drift rate of solids $v_{r\bullet}$, normalized by the Keplerian orbital speed, v_K , is given by the well-known expression (Nakagawa et al. 1986):

$$\frac{v_{r\bullet}}{v_K} = \frac{v_r - 2 \text{St} \eta v_K}{v_K (1 + \text{St}^2)}. \quad (10)$$

Importantly, this drift arises both from the accretionary flow of the gas (given by the first term in the numerator of the above expression), as well as from the head-wind experienced by the particles due to the sub-Keplerian flow of the gas. The latter effect depends on the magnitude of pressure support within the disk, and is controlled by the sub-Keplerian factor, η , which is approximately equal to the square of the disk's geometric aspect ratio (Armitage 2010). More specifically, for the disk-model at hand it is straightforward to show that $\eta = (51/40)(h/r)^2 \sim 3 \times 10^{-3}$. The radial profile of η is shown on the top panel of Fig. 4 with a pink line.

The absolute value of the normalized radial dust velocity $|v_{r\bullet}/v_K|$ is shown on the top panel Fig. 4 with a black curve.

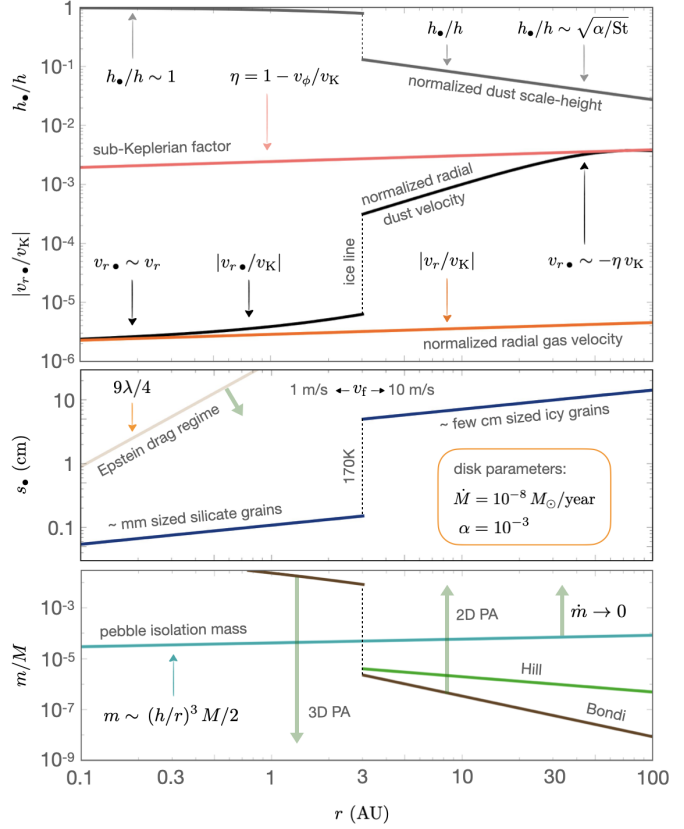


Fig. 4. Vertical thickness of the dust subdisk, radial drift of solids, particle size profile, and pebble accretion regimes in a fiducial ($\alpha = 10^{-3}$ and $\dot{M} \sim 10^{-8} M_{\odot} \text{ yr}^{-1}$) model disk. Owing to strong dust-gas coupling in the inner disk, the solid layer is well-mixed (such that $h_{\bullet} \sim h$) and experiences slow ($v_{r\bullet} \sim v_r$) inward drift. In the outer disk, dust settling is much more efficient, and the radial velocity of icy grains achieves a value comparable to its upper limit of $v_{r\bullet} \sim -\eta v_K$. The model further predicts that particle radii within the inner disk do not exceed the millimeter scale, while readily growing to sizes as large as a few centimeters beyond the ice line. The change in physical regimes of dust evolution across the water ice sublimation front translates to an important distinction in the modes of pebble accretion between the inner and outer regions of the nebula. While rapid 2D capture of solid dust can ensue in the outer disk for relatively low-mass protoplanetary embryos, the inner disk is fully confined to the comparatively inefficient 3D regime of pebble accretion.

As with the scale height of the solid subdisk, the ice-line plays an important role in separating the particle drift regimes. In the inner disk, dust drifts very slowly relative to Keplerian orbital speed and approaches the accretionary velocity of the gas (shown as an orange line). In the outer disk, particle drift due to head-wind dominates and for $r \gtrsim 40$ AU, as the stokes number tends to unity, the radial velocity approaches its maximal limit of $|v_{r\bullet}/v_K| \rightarrow \eta$.

While the Stokes number itself quantifies the strength of dust-gas coupling, it is important to keep in mind that fundamentally, St is set by the physical size of dust grains. Accordingly, we can employ the Epstein drag law⁵ to relate the Stokes number to the particle radius, s_{\bullet} :

$$\text{St} = \sqrt{\frac{\pi \rho_{\bullet}}{8 \rho} \frac{s_{\bullet}}{c_s} \Omega}. \quad (11)$$

⁵ This drag law is only appropriate for particles with radii smaller than or equal to $9/4$ times the mean free path of the gas molecules. We confirm the applicability of this regime a posteriori.

For the sake of definitiveness, we adopted particle densities of $\rho_* = 1 \text{ g/cc}$ and 3 g/cc for icy and rocky grains, respectively. The particle radius is shown as a function of stellocentric distance in the middle panel of Fig. 4. Interior to the ice-line, rocky grains possess characteristic radii on the order of a millimeter. Beyond the ice-line, however, our model predicts that icy particles can achieve radii of a few centimeters, even reaching a decimeter for $r \gtrsim 30 \text{ AU}$.

As a final result of this section, we consider the accretion of dust onto planetary objects, with an eye towards delineating the relevant physical regimes. Crudely speaking, accretion of solid dust ensues when planetary gravity can detach drifting particles from the background gaseous flow, causing the grain to spiral in towards the planet. Given a planetary mass, m , the characteristic length scale over which this can occur is the modified Bondi radius, $\mathcal{R}_B = \mathcal{G} m / (\eta v_K^2) \sqrt{St M \eta^3 / m}$, where the multiplicative factor within the square root accounts for the strength of dust-gas coupling (Lambrechts and Johansen 2012).

The rate of mass accretion itself further depends on whether the particle layer forms a thin subdisk or is vertically extended. In the former case, dust capture proceeds in a 2D regime at the rate $\dot{m}_{2D} = 2 \Sigma \sqrt{2 \mathcal{G} m r \eta} St$. Conversely, in the case of 3D accretion, the rate of planetary mass growth has the form $\dot{m}_{3D} = m \Sigma St \sqrt{2 \pi \mathcal{G} r^3 / M} / h_*$ (Ormel 2017). Equating these two expressions, the criterion for transition from 2D to 3D pebble accretion can be formulated as a critical planetary-to-stellar mass ratio:

$$\left(\frac{m}{M}\right)_{2D-3D} \sim \frac{4 \alpha \eta h^2}{\pi r^2 St (St + \alpha)}. \quad (12)$$

The RHS of this expression can be readily computed from results delineated in the proceeding text and the critical mass ratio is shown as a function of orbital radius in the bottom panel of Fig. 4 with a brown line. Once again, the ice-line plays a decisive role: interior to the water-ice sublimation front, the pebble accretion process lies firmly in the 3D regime. Conversely, beyond the ice-line, 2D accretion is ensured for sufficiently massive protoplanets, with the critical mass ratio decreasing with increasing stellocentric distance.

Beyond this 2D-3D boundary, there exists an additional transitional mass scale, pertinent to 2D accretion. In a regime where the Bondi accretion radius exceeds the Hill accretion radius $\mathcal{R}_H = r (10 St m / (3 M))^{1/3}$, the latter becomes the relevant pebble capture length-scale (Ida et al. 2016). This Bondi-Hill partition corresponds to a different critical mass scale, which can be computed by setting $\mathcal{R}_H \sim \mathcal{R}_B$:

$$\left(\frac{m}{M}\right)_{B-H} \sim \frac{100 \eta^3}{9 St}. \quad (13)$$

This relation is depicted as a dark green curve on the bottom panel of Fig. 4 and shows that within the context of our disk model, the transition from Bondi to Hill accretion in the outer disk ensues when the planetary mass becomes comparable the Earth-Mars range, depending on the orbital period.

With these analytic results in hand, it is important to keep in mind that planetary accretion is not a process that is fixed to a given orbital radius. Rather, disk-driven orbital decay can cause growing planets to migrate across the ice line, effectively halting their accretion process. Conversely, rapid outward migration of protoplanetary embryos facilitated by the thermal torque (Masset 2017; Guilera et al. 2019) can cause objects to enter a domain where bona fide 2D accretion can ensue. In other words,

the interplay between accretion and migration constitutes an important driver of emergent diversity within planetary systems.

Irrespective of the exact regime in which pebble accretion operates, planetary growth cannot continue without bounds. Rather, Lambrechts et al. (2014) have shown that the pebble accretion process is self-limiting, and naturally terminates when a planet reaches the pebble “isolation mass.” Notably, this mass-scale is related to the cube of the disk’s geometric aspect ratio and to within a factor of order unity, it is equal to the so-called “thermal mass” scale:

$$\left(\frac{m}{M}\right)_{iso} \sim \frac{1}{2} \left(\frac{h}{r}\right)^3. \quad (14)$$

The pebble isolation mass is shown in the bottom panel of Fig. 4 as a cyan line.

Cumulatively, our simple analysis points to a clear ranking of pebble accretion regimes that is strikingly different in the inner and outer regions of the disk. Interior to the ice-line, pebble accretion proceeds entirely in the 3D regime and is therefore comparatively inefficient. Exterior to the ice-line, the 3D regime of dust capture gives way to 2D Bondi accretion at low protoplanetary masses and switches to 2D Hill accretion as the planetary mass increases. These results suggest that while planets may readily reach the isolation mass through pebble accretion in the outer disk, a different mode of growth (i.e., pairwise collisions among planetesimals) is likely to dominate within the inner regions of protoplanetary nebulae.

5. Conclusion

In this work, we outline a simple model for the strength of dust-gas coupling within protoplanetary disks, as characterized by the Stokes number. The qualitative basis of our theoretical picture can be understood as follows. Through hydrodynamic drag, turbulent fluctuations within circumstellar nebulae excite the velocity dispersion among dust particles. In addition to being dependent upon the gas surface density and the magnitude of turbulent viscosity itself, the square of the dust velocity dispersion scales with Stokes number (Ormel & Cuzzi 2007).

While particle coagulation leads to larger values of St and an enhanced spread of particle velocities, collisional fragmentation – which is quantified by a composition-dependent threshold speed (Blum and Münch 1993) – serves as the limiting mechanism for the rise in St. Therefore, an equivalence between the dust velocity dispersion and the fragmentation speed yields an estimate for the maximum value of the Stokes number attainable by particles at a given orbital radius for a specified combination of disk parameters α and \dot{M} (Eq. (8); Fig. 3).

The key implications of our results are readily summarized. While the Stokes number exhibits an almost linear dependence on the orbital radius, a much more dramatic (factor of $\sim 10^2$) enhancement of St ensues across the water sublimation line, owing to an order-of-magnitude increase in the fragmentation velocity of the grains. For nominal disk parameters of $\alpha = 10^{-3}$ and $\dot{M} = 10^{-8} M_\odot \text{ yr}^{-1}$, the characteristic values of the Stokes number evaluate to $St \sim 10^{-4}$ (corresponding to a particle size of order a millimeter) and $St \sim 10^{-1}$ (corresponding to a particle size of a few centimeters) in the inner and outer regions of the disk, respectively. Because of this dichotomy, both vertical settling as well as radial drift of dust are likely to be efficient within the outer regions of protoplanetary disks⁶. Conversely, silicate

⁶ We note, however, that numerous mechanisms may act to trap dust locally, suppressing large-scale radial drift.

dust within inner regions of protoplanetary disks is expected to be vertically well-mixed and sink towards the host star at a rate comparable to the accretionary flow of the gas (see Fig. 4).

There are a number of avenues through which our model can be expanded upon. Perhaps most trivially, our “active disk” treatment of the energy balance can be extended to account for “passive” stellar irradiation as well as more realistic radiative transfer. Additionally, it is possible to consider radially variable accretion rates (Laibe et al. 2012) or incorporate non-viscous drivers of gas accretion, such as disk winds (Tabone et al. 2021), although this would complicate the relationship between \dot{M} and the surface density. As yet another example, the viscosity parameter itself can be endowed with a radial dependence (Penna et al. 2013), given that distinct modes of (magneto)hydrodynamic turbulence are expected to operate in different regions of the disk (Lyra and Umurhan 2019). Similarly, a more sophisticated treatment of the fragmentation threshold can be readily employed (Blum and Wurm 2008; Vericel & Gonzalez 2020), yielding additional radial structure within the Stokes number profile. Although each of these (and other) developments are undoubtedly worthwhile, it is unlikely that the principal results of our work will be altered dramatically. In other words, our determination that dust-gas coupling is taut in the inner disk and marginal beyond the ice-line is likely robust.

A number of physical processes, including the onset of the streaming instability as well as the accretion of pebbles, exhibit a pronounced dependence on the Stokes number, with higher values of St generally corresponding to faster growth (Yang et al. 2017; Ida et al. 2016). Despite the stark difference in characteristic Stokes number that ensues across the water-ice sublimation front, however, planetesimal formation is expected to operate efficiently in the inner and outer regions of the disk alike. In particular, assuming parameters similar to those derived herein (i.e., $s_{\bullet} \sim \text{mm}$ in the inner disk, $s_{\bullet} \sim \text{cm}$ in the outer disk,) a recent work by Morbidelli et al. (2021) has demonstrated how radial concentration of solids near the silicate and H_2O sublimation lines naturally leads to the contemporaneous generation of rocky and icy planetesimals through gravito-hydrodynamic instabilities (see also Drążkowska et al. 2016; Izidoro et al. 2021).

Growth beyond the planetesimal stage, however, is a different matter. While our results indicate that capture of pebbles can drive rapid accretion of protoplanets beyond the ice-line (Lambrechts and Johansen 2012), the low value of the Stokes number in the inner disk indicates that accretion of silicate pebbles is markedly inefficient. Therefore, pairwise collisions among planetesimals likely constitute the dominant process through which rocky planets coalesce (Hansen 2009). This difference in growth modes stems primarily from the fact that pebble accretion in the inner disk is expected to proceed in the (slow) 3D regime, whereas the vertical settling of grains in the outer disk allows for a rapid accumulation of icy dust through 2D pebble accretion. Our results thus indicate that beyond constituting a partition in the chemical composition of solids, the ice-line

represents a veritable divide in physical accretion regimes and thus plays a decisive role in sculpting the large-scale architecture of planetary systems.

Acknowledgments. We thank the anonymous referee for providing a thorough and insightful referee report. K.B. is grateful to Caltech, Observatoire de la Côte d’Azur, the David and Lucile Packard Foundation, and the National Science Foundation (grant number: AST 2109276) for their generous support. A.M. acknowledges support from the ERC advanced grant HolyEarth N. 101019380.

References

Adachi, I., Hayashi, C., & Nakazawa, K. 1976, *Prog. Theor. Phys.*, **56**, 1756

Armitage, P. J. 2010, *Astrophysics of Planet Formation, Astrophysics of Planet Formation*, ed. Philip J. A. (Cambridge, UK: Cambridge University Press), 294, 2010

Bell, K. R., & Lin, D. N. C. 1994, *ApJ*, **427**, 987

Birnstiel, T., Dullemond, C. P., & Brauer, F. 2009, *A&A*, **503**, L5

Birnstiel, T., Klahr, H., & Ercolano, B. 2012, *A&A*, **539**, A148

Bitsch, B., Morbidelli, A., Lega, E., & Crida, A. 2014, *A&A*, **564**, A135

Bitsch, B., Raymond, S. N., & Izidoro, A. 2019, *A&A*, **624**, A109

Blum, J., & Münch, M. 1993, *Icarus*, **106**, 151

Blum, J., & Wurm, G. 2008, *ARA&A*, **46**, 21

Chiang, E., & Youdin, A. N. 2010, *Ann. Rev. Earth Planet. Sci.*, **38**, 493

Drążkowska, J., Alibert, Y., & Moore, B. 2016, *A&A*, **594**, A105

Dubrulle, B., Morfill, G., & Sterzik, M. 1995, *Icarus*, **114**, 237

Guilera, O. M., Cuello, N., Montesinos, M., et al. 2019, *MNRAS*, **486**, 5690

Hansen, B. M. S. 2009, *ApJ*, **703**, 1131

Hartmann, L., Calvet, N., Gullbring, E., & D’Alessio, P. 1998, *ApJ*, **495**, 385

Hayashi, C. 1981, *Prog. Theor. Phys. Suppl.*, **70**, 35

Ida, S., Guillot, T., & Morbidelli, A. 2016, *A&A*, **591**, A72

Izidoro, A., Dasgupta, R., Raymond, S. N., et al. 2021, *Nat. Astron.*, **6**, 357

Johansen, A., & Youdin, A. 2007, *ApJ*, **662**, 627

Kokubo, E., & Ida, S. 2012, *Prog. Theor. Exp. Phys.*, **2012**, 01A308

Laibe, G., Gonzalez, J.-F., & Maddison, S. T. 2012, *A&A*, **537**, A61

Laibe, G., Bréhier, C.-E., & Lombart, M. 2020, *MNRAS*, **494**, 5134

Lambrechts, M., & Johansen, A. 2012, *A&A*, **544**, A32

Lambrechts, M., Johansen, A., & Morbidelli, A. 2014, *A&A*, **572**, A35

Lambrechts, M., Morbidelli, A., Jacobson, S. A., et al. 2019, *A&A*, **627**, A83

Lee, U., Osaki, Y., & Saio, H. 1991, *MNRAS*, **250**, 432

Lynden-Bell, D., & Pringle, J. E. 1974, *MNRAS*, **168**, 603

Lyra, W., & Umurhan, O. M. 2019, *PASP*, **131**, 072001

Masset, F. S. 2017, *MNRAS*, **472**, 4204

Morbidelli, A., Baillié, K., Batygin, K., et al. 2021, *Nat. Astron.*, **6**, 72

Musiolik, G., & Wurm, G. 2019, *ApJ*, **873**, 1

Nakagawa, Y., Sekiya, M., & Hayashi, C. 1986, *Icarus*, **67**, 375

Ormel, C. W. 2017, *The Emerging Paradigm of Pebble Accretion*, Formation, Evolution, and Dynamics of Young Solar Systems (Berlin: Springer), 445, 197

Ormel, C. W., & Cuzzi, J. N. 2007, *A&A*, **466**, 413

Ormel, C. W., & Klahr, H. H. 2010, *A&A*, **520**, A43

Penna, R. F., Sądowski, A., Kulkarni, A. K., & Narayan, R. 2013, *MNRAS*, **428**, 2255

Pillich, C., Bogdan, T., Landers, J., Wurm, G., & Wende, H. 2021, *A&A*, **652**, A106

Shakura, N. I., & Sunyaev, R. A. 1973, *A&A*, **24**, 337

Stewart, S. T., & Leinhardt, Z. M. 2009, *ApJ*, **691**, L133

Tabone, B., Rosotti, G. P., Cridland, A. J., Armitage, P. J., & Lodato, G. 2021, *MNRAS*, **512**, 2290

Vericel, A., & Gonzalez, J.-F. 2020, *MNRAS*, **492**, 210

Weidenschilling, S. J. 1977, *MNRAS*, **180**, 57

Yang, C.-C., Johansen, A., & Carrera, D. 2017, *A&A*, **606**, A80

Youdin, A. N., & Goodman, J. 2005, *ApJ*, **620**, 459.